Complément à l'article http://dx.doi.org/10.52497/jitipee.v9i1.390

Arc cathode interaction modelling in the case of a non refractory cathode material

Arthur Monnoyer, Pierre Freton, and Jean-Jacques Gonzalez

Abstract *- Modeling phenomena related to the interaction of electric arcs with electrodes allows, on the one hand, to complete the magnetohydrodynamic models usually employed to represent the column, by providing useful boundary conditions, and on the other hand to study the heating and erosion of these electrodes. This modeling is complex due to the large number of phenomena that should be accounted for, and to the deviations from local thermodynamic equilibrium (LTE) caused by the small distances involved. An important issue is therefore to understand how these deviations to LTE structure the near-electrode zone, particularly in the less-studied case of a non-refractory cathode. This article presents, based on the literature, a methodology to evaluate the characteristic lengths of appearance of thermal, chemical (ionization), and charge separation imbalances. This methodology is validated on the well-known case of argon plasma under 1 bar, and is then applied to a copper plasma under high pressure (28 bars) resulting from the vaporization of a copper (non-refractory) cathode subjected to an arc. The results of the study confirm the cathode zone structures established by Benilov, and in particular the presence of ionization in the sheath associated with the copper cathode. A self-consistent cathode layer model taking into account these phenomena is then presented, and applied to the calculation of a structure with N stationary and independent cathode spots. In the case of an arc attached to the hollow (copper) cathode of a high-power plasma torch, good orders of magnitude are obtained for the sheath voltage and the vaporization erosion rate. To conclude, study perspectives on this subject are proposed.*

Key words: *electric arc, cathode spots, nonequilibrium plasma model, space charge sheath*

1. Introduction

Understanding the interactions between an electric arc and its environment, and particularly metallic materials, is the subject of numerous studies due to its industrial interest [1, 2]. At atmospheric pressure, examples include the cathodes and anodes of plasma torches used for welding, cutting, thermal spraying, or waste treatment. This issue is also central to the understanding of spot phenomena observed in particular on vacuum arc cathodes [3, 4], used for example in medium voltage circuit breakers.

In order to better understand the phenomena related to the presence of the electric arc in these processes (with the aim of improving them), their modeling is of particular importance. Among the available approaches, magnetohydrodynamic (MHD) models with local thermodynamic equilibrium (LTE) assumption are widely used to predict gas flows in the presence of an electric arc [5, 6]. One of the limitations of this approach is the consideration of electrode phenomena, because they are located on a very small scale. On the one hand, this implies deviations from LTE [7, 8], the various equilibria having 'not enough time' to establish. Departures from thermal and chemical equilibrium, and deviations from neutrality (presence of sheaths) must therefore be taken into account. On the other hand, the numerical treatment of these small scales would involve considering a very refined mesh, and would therefore lead to particularly expensive calculations.

Physically, a central problem of arc-electrode interaction is that of current continuity: the mechanisms of charge transfer in the arc bulk (LTE conductivity) are very different from those at the interface with the electrode (electron emission and ion flux at the cathode, collection of thermal electrons at the anode, etc.). This raises the problem of constructing boundary conditions for the plasma (particularly concerning current density) that account for these electrode phenomena. Once obtained, these boundary conditions can (in principle) be applied to the MHD model. Another interest of studying this interaction is to be able to predict the heating of the electrodes by the non-equilibrium plasma layer, and thus, if necessary, their erosion by melting and vaporization.

We will focus more specifically on the modeling of the arc-cathode interaction. This subject is known for its difficulty, due on the one hand to the numerous phenomena to be taken into account and their couplings, and on the other hand to the lack of experimental data to validate the models. Thus, many models have been proposed (see for example [8-10] and references therein to get an idea), often with drastic simplifications, and it is difficult to identify the relevant elements provided by each model. Faced with this observation, it seems reasonable to turn to theoretical approaches with clear physical content, valuing self-consistency, and minimizing the number of hypotheses or *ad hoc* parameters.

Among the approaches claiming these advantages, the work of Benilov's team summarized in [2, 8] has significantly contributed to improving the understanding of refractory cathodes subjected to an arc established in an ambient gas. In particular, the case of the argon-tungsten system has been extensively studied [11-14]. This choice is probably due to the abundance of available data necessary for the description of the non-equilibrium argon plasma (cross sections, ionization coefficient, etc.).

Non-refractory cathodes (e.g. copper), although studied for more than 60 years, remain less understood than their refractory counterparts. When operating in the electric arc regime, these cathodes undergo significant vaporization in small unsteady structures called 'cathode spots' [3]. In vacuum, these spots have a radius of the order of 10 µm, and evolve over times of the order of 10 ns. The extreme conditions (temperatures of about 4000 K, vapor pressures exceeding 20 bars) coupled with the small scales make experimental studies extremely delicate, and the uncertainties on the results are usually counted in orders of magnitude [4]. This difficulty in obtaining quantitative experimental results obviously poses a problem for the validation of models. This explains the very large number of theoretical approaches proposed in the literature to model these spots. On this subject, a fairly comprehensive review of 'historical' work (prior to 1990) presented in [10] concludes that the large number of published models contributes more to confusion than to a better understanding of the phenomena. While the 'ingredients' of modeling the cathode zone (vaporization, electron emission, ionization, charge and energy balances, etc.) are well identified, there remain many disagreements on the formulation to adopt.

Papers [15-18] address the modeling of non-refractory cathodes by following an approach similar to that developed by Benilov for refractory cathodes. Note also that [18] aims to reconcile the two types of approaches (evaporative and explosive, cf. [10]) which, historically, were developed separately for the modeling of spots. It seems reasonable to rely on these works, which use the same self-consistency approach than that adopted for refractory cathodes.

In this paper, we first review the deviations to LTE present in the vicinity of a wall. The two types of cathodes (refractory or not) are then presented and characterized, as well as the structures of the

associated cathode zones. The latter are obtained in light of the length scales characterizing non-equilibrium phenomena. Based on the formulation established in [16], a cathode spot model is introduced. The model is able to predict sheath voltages and erosion rates, which can be compared to experimental data. Finally, perspectives for improving existing models are presented, particularly concerning unsteady phenomena.

2. Deviations to LTE in the vicinity of a wall

As mentioned in the introduction, the LTE state is disturbed in the vicinity of the electrodes due to the evolution of phenomena over small distances. In order to characterize these deviations from LTE, Benilov [2, 19] has proposed expressions for the characteristic lengths of appearance of these phenomena in the vicinity of the electrodes. The characterization of these lengths in the conditions of interest makes it possible to know whether these phenomena should be treated simultaneously, or can on the contrary be treated successively within well-separated 'layers'. We thus define:

- The thermalization length λ_{th}, characterizing the thermal imbalance between electrons and heavy particles, which then have two different temperatures (denoted T_e and T_h in the following). This balance is in principle ensured by the elastic collision energy transfer between electrons and heavy particles. However, in the vicinity of a wall, it can be disturbed by the thermal conduction of heavy particles, which evacuates the energy deposited by the electrons. The thermalization length is then precisely the scale at which these two processes enter into competition.

- The mean free paths $\lambda_{\alpha\beta}$ of collisions between particles of species α and β, which are the average distances between two collisions of this type.

- The Debye length λ_D, which characterize of the screening of the electric field existing at the cathode to regulate the particle fluxes.

- The ionization length λ_{ion}, characterizing the ionization nonequilibrium of the plasma, i.e. the deviations from Saha's law. These are due to the fact that an atom emitted by vaporization or desorption will 'survive' for a certain time τ before undergoing its first ionization by an electron. Since it moves at a certain average velocity v, it will travel a distance $\lambda_{ion} = v\,\tau$ (the ionization length) during its lifetime. Thus, at length scales smaller than λ_{ion}, ionization equilibrium cannot be established because very few ionization reactions take place. Depending on whether the dynamics of the atom preceding its ionization is collisional or not (which affects its average velocity v), there are two expressions for this length. The collisional ionization length will be noted λ_{ion}^{d} (v will then correspond to a diffusion velocity), its non-collisional version will be noted λ_{ion}^{nc} (v will then correspond to a thermal velocity).

We refer to Appendix A for a summary of the basic expressions and useful data for calculating these lengths. Examples of numerical applications under conditions of interest for our study are presented in Section 3.2.

Complément à l'article http://dx.doi.org/10.52497/jitipee.v9i1.390

3. Refractory and non-refractory cathodes

3.1. Classification

When a metal is placed in a vacuum and heated, it tends to emit electrons (thermionic emission phenomenon) and neutral atoms (vaporization phenomenon). Depending on the predominance of the emitted particles, metals used as cathodes for electric arcs are usually classified into two categories, illustrated in Figure 1:

- Refractory cathodes which, when heated in a vacuum, emit more electrons by thermionic emission than atoms by vaporization. For this to be possible, the material must be able to be heated to a high temperature (above 3000 K) without undergoing significant evaporation. Examples of refractory cathodes are those made of tungsten or hafnium.

- Non-refractory cathodes which, when heated in a vacuum, emit more atoms by vaporization than electrons by thermionic emission. Non-refractory cathodes are often made of a material with a 'low' melting point, a typical example being copper.

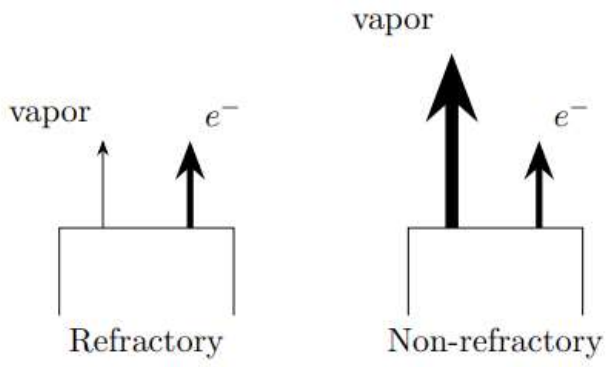

Figure 1 : Two types of cathodes depending on the predominance of emitted particles

For a more quantitative distinction, we can compare the vaporization energy $m_a L_{vap}$ (m_a being the mass of an atom and L_{vap} the latent heat of vaporization) to the work function W. The cathode will then be refractory if $W < m_a L_{vap}$ (i.e., if it is easier to extract electrons than atoms). For example, copper and tungsten both have a work function of about 4.5 eV, but copper has a vaporization energy of 3.1 eV, while that of tungsten is 8.5 eV. Thus, a tungsten cathode is refractory, but a copper cathode is not.

3.2. Cathode zone structures

It is useful to understand the structure of the cathode zone in terms of the presence or absence of nonequilibrium phenomena. To do this, we will use the characteristic lengths presented in section 2. For example, if the Debye length is small compared to all the other characteristic lengths, it will be possible to separate the cathode zone into 2 regions: a sheath without collisions or ionizations in which the deviations from neutrality are localized, and a "pre-sheath", which will be quasi-neutral, but within which the other nonequilibrium phenomena will be present. Thus, the characterization under the conditions of refractory and non-refractory cathodes of the length scales seen previously makes it possible to understand the structures of the associated cathode zones.

Since a refractory cathode undergoes little vaporization, it is most often considered to be in direct contact with the ambient plasma (metal vapors from the electrode are then neglected). A classic case is that of argon plasma under atmospheric pressure. To illustrate, Figure 2 presents, for these plasma conditions, the numerical calculations of the length scales previously introduced.

We can see from this figure that, whatever the temperature T_e, we have $\lambda_D << L$, with $L = \lambda_{ion}, \lambda_{\alpha\beta}, \lambda_{th}$. Note that for ion-ion collisions, we only have $\lambda_D < \lambda_{ii}$. However, we will assume a non-collisional sheath, which can be justified [19]. Under these conditions, it is possible to separate the (non-collisional) sheath from the rest of the cathode zone (pre-sheath). Note also that $\lambda_{ia} < \lambda_{aa}$, which comes from the large charge exchange cross-section assumed to dominate ion-atom collisions. The very rapid increase of λ_{aa} with T_e is due to ionization, which tends to decrease the density of atoms. The inequality $\lambda_{ia} < \lambda_{aa}$ allows us to assume that atoms diffuse into ions. Finally, depending on the values of T_e, the atoms in the ionization zone characterized by the lengths λ_{ion} are either collisional ($T_e < 35000$ K, $\lambda_{ia} < \lambda_{ion}^{d}$), or non-collisional ($T_e > 35000$ K, $\lambda_{ia} > \lambda_{ion}^{nc}$). In this regard, the point of intersection between λ_{ia}, λ_{ion}^{d} and λ_{ion}^{nc} at $T_e \sim 35000$ K is satisfying.

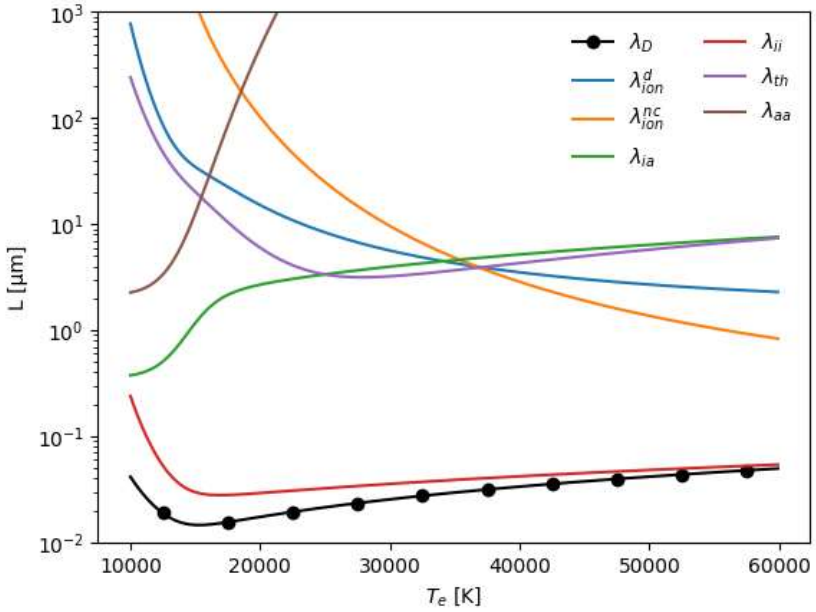

Figure 2 : Characteristic length scales of apparition of diverse non-equilibrium phenomena for an argon plasma. P = 1 bar, T_h = 3000 K.

Under these conditions, the physics of the cathode zone for a refractory material is relatively well understood. In particular, the so-called *Near Cathode Plasma Layer* (NCPL) model developed about twenty years ago by Benilov's team [11, 20, 21] is based on clear physical foundations and has been experimentally validated [22]. A summary of the model is presented in [23], and an implementation is available online [24]. More recently, it has been shown that it is possible to couple this model to a description of the plasma in LTE in simple geometries with a fixed arc root, in steady state [13, 14], or unsteady state [25, 26], thus providing relevant boundary conditions for this type of cathode, both to the plasma and to the material.

In contrast, the physics of non-refractory cathodes is still poorly understood, and will therefore be the main subject of this article. To emit electrons, such a cathode must rise to a temperature higher

than its vaporization temperature, which causes the appearance of a very high vapor pressure on its surface. To estimate this pressure p_{vap}, we can use the Clausius-Clapeyron formula:

$$p_{vap}(T_w) = \frac{p_{ref}}{2} \exp\left(\frac{L_{vap} m_a}{k} \left(\frac{1}{T_{ref}} - \frac{1}{T_w} \right) \right) \quad (1)$$

where T_w is the surface temperature, L_{vap} is the latent heat of vaporization of the material, k is the Boltzmann constant, m_a is the mass of an atom, and (p_{ref}, T_{ref}) is a reference point (e.g., if p_{ref} = 1 atm, T_{ref} is the vaporization temperature). The (unusual) 1/2 factor comes from the fact that the emitted vapor distribution is assumed to be *semi*-Maxwellian, and therefore contains half as many particles as the equilibrium distribution referred to by the 'usual' Clausius-Clapeyron formula. Taking the example of a copper cathode, and assuming that the cathode temperature reaches 4000 K, the vapor pressure is estimated at 28 bars. The characteristic lengths of a copper plasma at 28 bars are therefore shown in Figure 3.

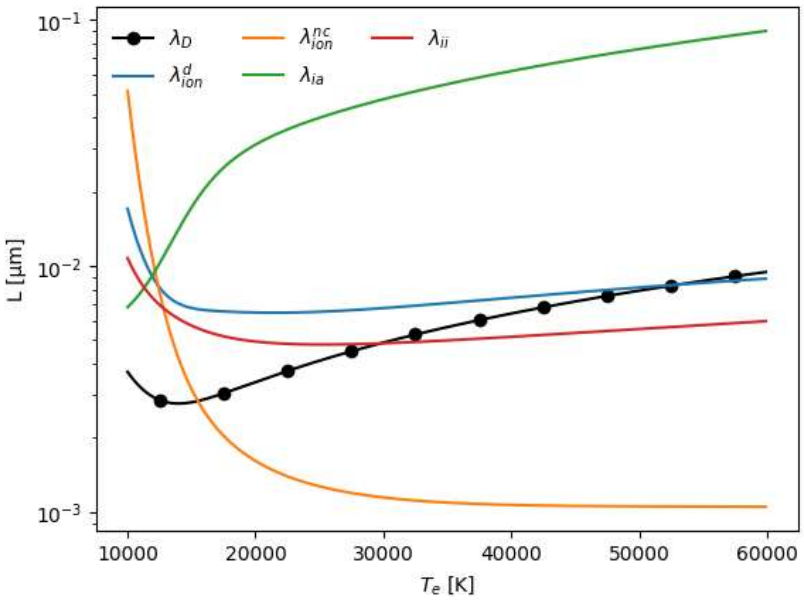

Figure 3 : Characteristic length scales of apparition of diverse non-equilibrium phenomena for a copper plasma. P = 28 bar, T_h = 4000 K.

Unlike in the case of refractory cathodes, the Debye length is not always small compared to other lengths, and in particular the ionization length λ_{ion}^{nc} (ionization always takes place in the non-collisional regime in this case). When $\lambda_{ion}^{nc} < \lambda_D$, this means that ionizations take place *in the sheath*, and not beyond. A cathode zone model for a non-refractory cathode must therefore be a sheath model *with ionization*. An example of such a model is discussed in the next section.

To conclude this section, let us note that these calculations, although very useful, present certain questionable aspects. For example, the species densities are calculated under hypotheses of chemical equilibrium, Maxwellian distributions and neutrality. However, the characterizations of length scales show precisely that these hypotheses are not always verified. For example, for the refractory cathode, calculating the Debye length at ionization equilibrium appears *a posteriori* inconsistent, given that it is on a scale smaller than the ionization length.

4. A cathode layer model for a non-refractory material

4.1. Model description

In order to model the phenomena occurring in the vicinity of the cathode under the conditions of a non-refractory material, we have taken up and re-developed the model proposed by Almeida et al. [16]. The main objective of this model is to calculate the characteristics of the sheath (electron temperature T_e, current density j, heat flux density q, mass flux density g, etc.) as a function of the surface temperature T_w and the sheath voltage U. Note that the temperature T_e is assumed to be uniform throughout the cathode zone. We thus obtain dependencies $j(T_w, U)$, $q(T_w, U)$ and $g(T_w, U)$. In order not to make the presentation too long, we prefer gathering all the equations of the model in Appendix B and refer to the original article [16] for the construction of these equations. Some basic data that is not presented explicitly in [16] are also given in Appendix A.

The stationary model [16] is decoupled from the ambient plasma. This is because the power deposited in the cathode zone greatly exceeds that coming from the plasma (e.g. in the form of conductive flux). As a result, the energy transfer even takes place in the other direction: it is the cathode zone that heats the ambient plasma and not the other way around.

The model [16] is based on the results of Benilov and Benilova [15] who numerically solved a sheath model with ionization. In the framework of this one-dimensional model [15], the Poisson equation, allowing the calculation of the electric potential in the sheath (non-neutral region) is coupled to a simple kinetic model describing the ionization by electron impact of the metallic vapor emitted by the cathode. The resolution shows that the electric potential profile is non-monotonic, and has the typical appearance shown in Figure 4.

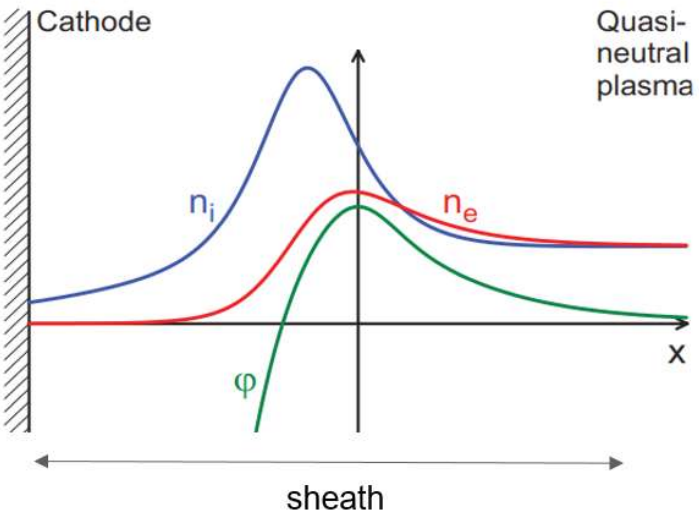

Figure 4 : Typical behaviour of the potential and charged particle densities calculated by the model [15]

In the model of Almeida et al. [16], the potential profile is taken into account in a simplified way, thanks to its maximum value and its average values to the left and right of the maximum. Figure 5 shows the main particle fluxes existing in the sheath.

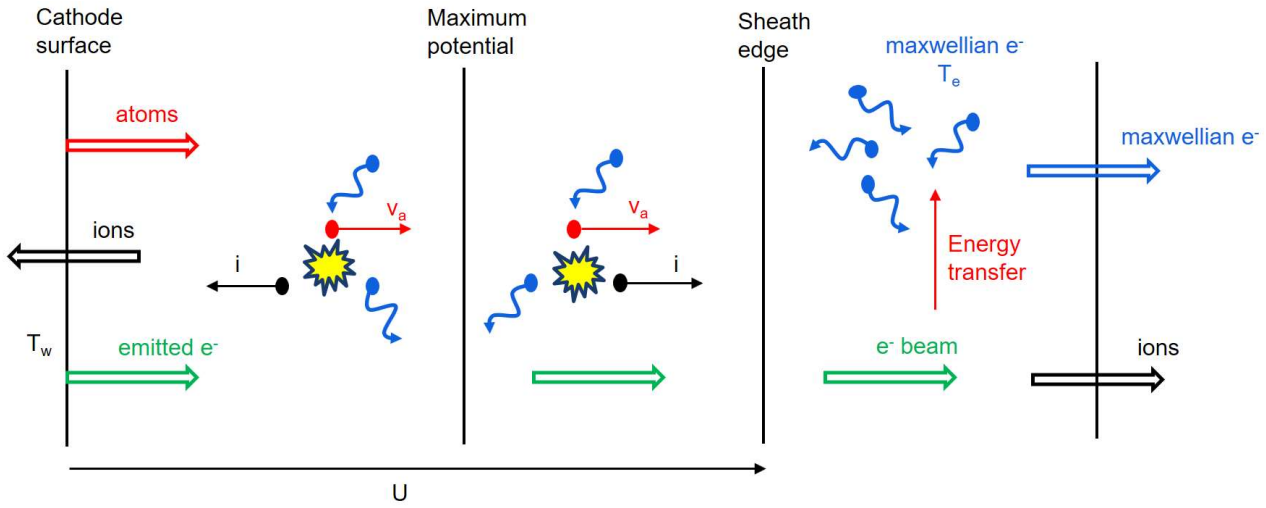

Figure 5 : Illustration of the main processes involved in the sheath. The 'explosions' (in yellow) represent ionizations.

A flux of atoms emitted by the cathode is calculated by the Langmuir formula. These atoms are then (partially) ionized in the sheath by electron impact with the Maxwellian electrons of the plasma. The ions thus generated to the left of the maximum potential are accelerated towards the cathode, which then receives an ion current actively participating to its heating. The ions generated to the right of the maximum are accelerated towards the plasma, thus constituting a mass loss for the 'cathode + sheath' system. These ionizations also generate electrons that are added to the Maxwellian electrons of the plasma. Note that the model neglects the presence of multiply charged ions, which are assumed to form in the plasma beyond the sheath (they are then filtered by the potential maximum), and therefore are not part of the system studied.

The cathode, in addition to being heated to a high temperature, is also subjected to the intense space charge electric field generated by the charge imbalance in the sheath (see Figure 4). It therefore emits electrons on the one hand by thermionic emission, and on the other hand by field electron emission. In order to describe these phenomena, we used the Murphy-Good equation [27] giving the flux of emitted electrons according to the temperature T_w and the electric field E_w at the surface. This equation is widely used in the literature related to the electron emission of arc copper cathodes in vacuum [9], and in particular in the model [16]. Electron emission, in addition to contributing significantly to the electric current density, plays an essential role in energy balances. On the one hand, this emission cools the cathode (at low temperature, we can possibly have heating by the Nottingham effect described in [28] and taken into account in the model), and on the other hand, these electrons acquire energy after acceleration by the sheath voltage U, and transfer this energy to the Maxwellian electrons of the plasma by elastic collisions, thus actively participating in the heating of this electron gas (necessary to carry out the energy-costly ionizations).

In order to determine the electron temperature T_e and thus close the model (U and T_w being given), a global energy balance of the Maxwellian electrons in the sheath is considered; we refer to [16] for its construction and to Appendix B for its expression. It consists in balancing the source terms due to the work of the electric field and to the heating by the emitted electron flux, and the losses due to ionizations and to the electron flux leaving the sheath either on the plasma side or on the cathode side (backscattered electrons).

Once the electron temperature is determined, it is possible to calculate all the particle fluxes in the sheath, and in particular to deduce the functions $j(T_w, U)$, $q(T_w, U)$ and $g(T_w, U)$ mentioned previously. Finally, note that depending on the thermodynamic conditions (pressure, temperatures), the first ionization equilibrium (established at the sheath edge) sometimes corresponds to a partially ionized situation. Thus, ω factors representing the average charge of the heavy elements (atoms and ions, $\omega \leq 1$) must be taken into account. It should be noted that, although these factors are mentioned in [16], their locations in the equations are not much explained. We refer to Appendix B where the ω factors appear clearly.

4.2. Multiple solutions to the electron energy balance

Let us apply the model described above to the case of a copper cathode. Let us begin by noting that, for certain values of U and T_w, the equation for the energy balance of electrons with unknown T_e (equation (30) in Appendix B) has several solutions. Such an example is presented in Figure 6 for the case where U = 20 V and T_w = 3900 K.

In that case, the characteristics of the sheath $f(T_w, U)$ are multivalued, which poses two difficulties. On the one hand, a physical difficulty: that of choosing the relevant solution to return to a single-valued characteristic. On the other hand, that of obtaining the numerical solution of the balance, made more complex due to the existence of these multiple solutions.

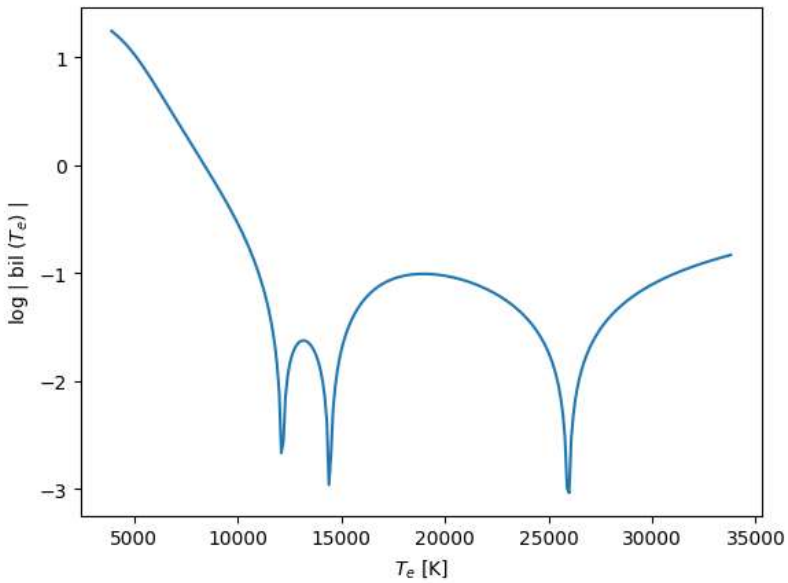

Figure 6 : Multiple solutions to the electron energy balance equation. U = 20 V, T_w = 3900 K

Thus, to plot the characteristics $f(T_w, U)$, it is necessary to treat the electron energy balance as the equation of an implicit curve $B(T_w, T_e) = 0$ in the temperature plane (T_w, T_e). A classical method for plotting this type of curve is presented in Appendix C. The sheath characteristics $f(T_w, U)$ can then be obtained using the following algorithm:

1) U is given (e.g. U = 20 V) and the position in the (T_w, T_e) plane is initialized to (5000K, 60000 K)
2) A first point on the curve $B(T_w, T_e) = 0$ is obtained using Newton's method described in Appendix C (step 1).

3) While $T_w > 2000$ K, the implicit curve $B(T_w, T_e) = 0$ is plotted for the given value of U, which gives triplets (U, T_w, T_e)
4) For each of those triplets, the particle fluxes, and in particular the functions j, q, and g are calculated and the data obtained is stored in a file.

Figure 7 thus presents a plot of the 'function' $T_e(T_w, U)$ for various sheath voltages U.

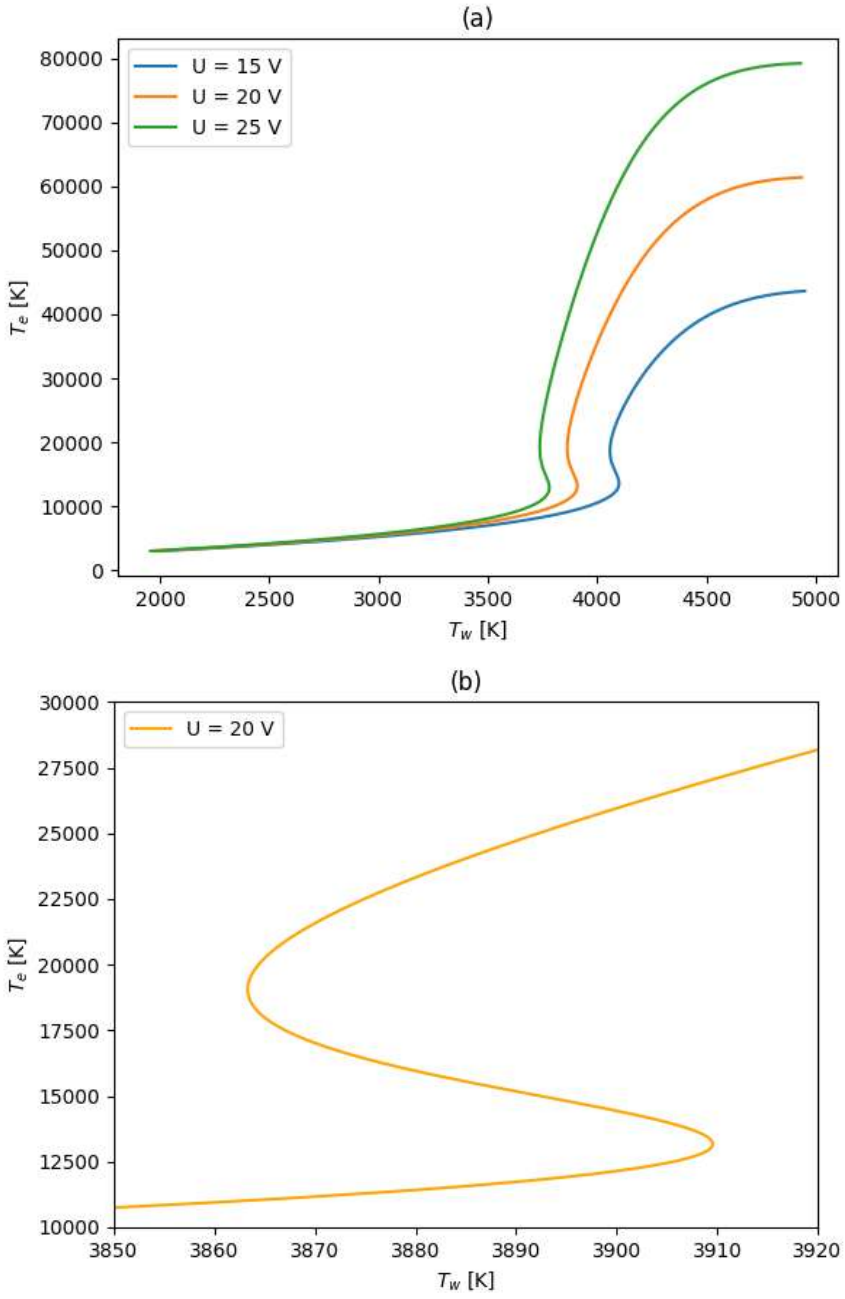

Figure 7 : Multivalued characteristics $T_e(T_w, U)$. (a) complete curve, (b) zoom on the retrograde section.

For each of these 'functions', we observe the existence, over a localized temperature range (around $T_w = 3900$ K for U = 20 V), of a 'retrograde section' connecting two branches that we will call low and high (referring to the values of T_e). The existence of this retrograde section was conjectured in

[16], but the latter had not been calculated at the time. It can be noted that its location in temperature T_w differs slightly from that anticipated in [16]. Let us now concentrate on the heat flux curves $q(T_w, U)$, represented in Figure 8.

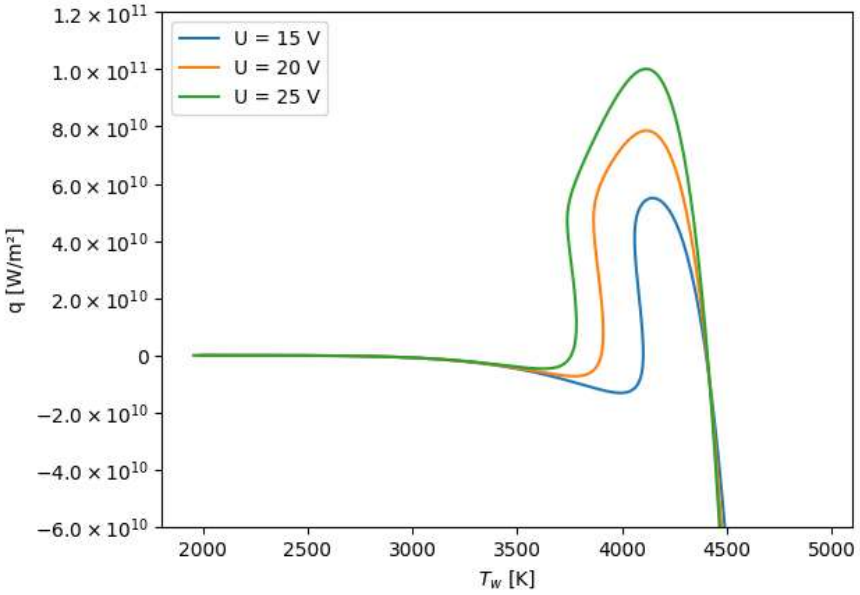

Figure 8 : Multivalued characteristics $q(T_w, U)$

In this figure, we find domains corresponding to the low and high temperature branches identified previously. The general appearance of these curves is very similar to that obtained (with a different model) for refractory cathodes. The decreasing part of the high branch (for $T_w > 4000$ K) is particularly interesting because it allows stable operation of a heating structure (the flux decreasing if the temperature increases and vice versa). The existence of this decreasing section motivates the choice, which we will adopt, of keeping only the high branch for the calculation of the heating of the cathode. It would however be interesting to analyze more in depth the physics behind these multivalued curves in future work (particularly the retrograde section).

4.3. Single-valued characteristics

Having made the choice to keep only the upper branch, it remains to design an efficient algorithm (more efficient than the implicit curve tracing) to obtain the characteristics $f(T_w, U)$ corresponding to this choice. For this, the key step is to detect the turning point marking the end of the upper branch. Once this point is determined, the electron energy balance can be solved by the 'usual' Newton method, focusing on the upper branch in the case of multiple solutions. The resolution algorithm is then as follows:

1) U is given (e.g. U = 20 V), and a preliminary calculation is performed using the implicit curve tracing algorithm to detect the 'turning point' temperature T_w^r.
2) The temperature T_w is initialized at 5000 K
3) While $T_w > T_w^r$, one solves the electron energy equation focusing on the upper branch solution. Decreasing T_w by 10 K each step, we obtain as before triplets (U, T_w, T_e).
4) When $T_w \sim T_w^r$, the solution is 'manually' switched to the unique low T_e solution.
5) The calculations of triplets (U, T_w, T_e) is then continued until $T_w = 2000$ K, lowering T_w by 10 K each step.

6) For each of the triplets obtained, the particle fluxes, and in particular the functions j, q, and g, are calculated and the results are stored in a file.

To detect the turning point, one could alternatively work with a smaller step of T_w, and impose a criterion on the slope of f(T_w, U).

For example, we obtain the characteristics j, q, and g represented in figures 9.

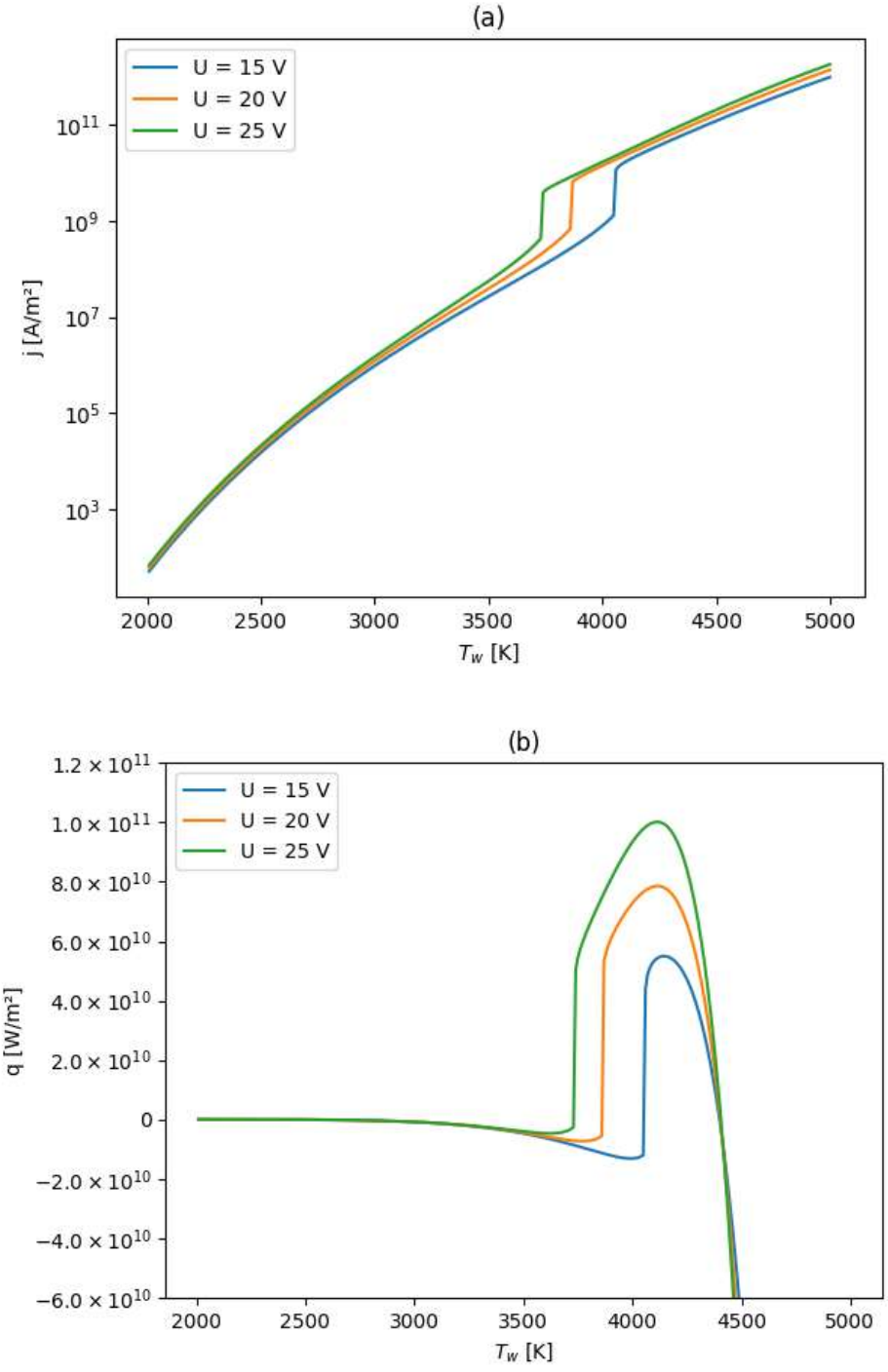

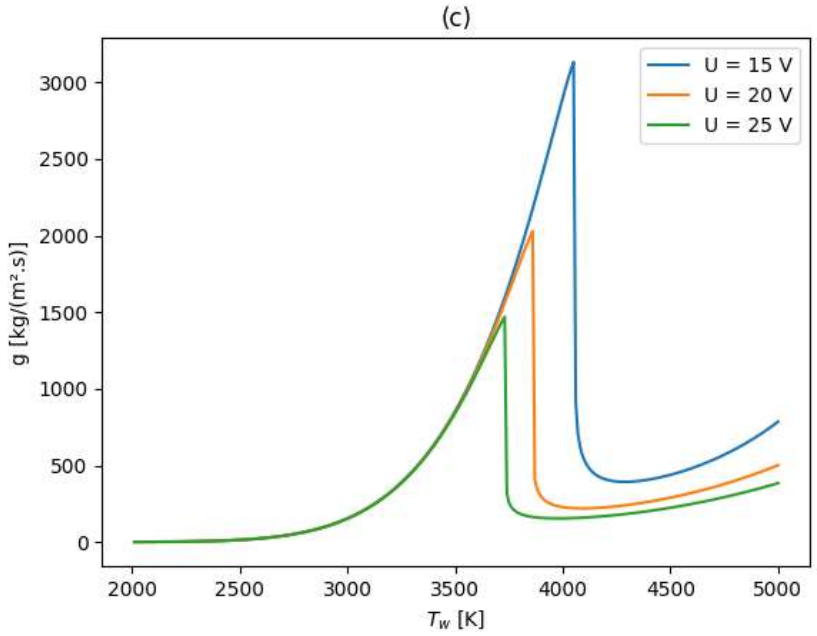

Figure 9 : Single-valued characteristics f(T_w, U). (a) f = j, (b) f = q, (c) f = g

These results are in excellent agreement with those presented in [16].

4.4. Physical discussion

We can note that the current density shows an exponential growth with the surface temperature for a given sheath voltage. This very rapid growth is due in particular to the exponential dependencies of the emitted current density. The jump at $T_w \sim 3700$ K is due to the solution branch change for the electron energy equation. This change results in a jump in the electron temperature T_e, which is reflected in the other calculated quantities, and in particular the current density.

The curve giving the heat flux q(T_w, U) is more delicate to interpret. First, note that before the jump in T_e, the value of the heat flux is negative. This negative value reflects cooling, mainly by vaporization. Once the jump is made, heating by ion bombardment has become very significant, due to more marked ionization at higher T_e, which explains the jump in heat flux q. If the surface temperature is further increased, cooling by electron emission eventually takes over, which explains the existence of a maximum for this flux, then its very rapid decrease.

Regarding the curve giving the mass flux g(T_w, U), it may seem surprising that this flux 'collapses' when moving to the solution at 'high' T_e. This is due to a very significant ionization of the emitted atoms before the maximum potential, which is consistent with the very high ion flux heating the cathode. Thus, these emitted then ionized atoms return to the cathode, and therefore do not constitute a mass loss for the latter. Note that the mass flux is higher at lower sheath voltage. It is likely that this behavior is due to a lower ionization (in particular before the maximum potential) when the sheath voltage is smaller.

5. Calculation of a N-spot structure

In this section, we want to describe the arc attachment on a non-refractory cathode. In the case of a vacuum arc, this attachment often appears as several (N > 1) cathode spots scattered over the

surface of the material. At atmospheric pressure, these spots tend to group together to form a macroscopic arc root. In the latter case, the arc root is often displaced, and the cathode material cooled down, so that the macroscopic arc root has an average temperature T_0. This temperature T_0 reflects, for example, cathode heating processes located on a larger scale than the spots. It can also represent an averaged effect of the N-1 other spots on which the temperature field of a given spot will be superimposed. This superposition then makes it possible to study the spots independently of each other. This situation is illustrated in Figure 10.

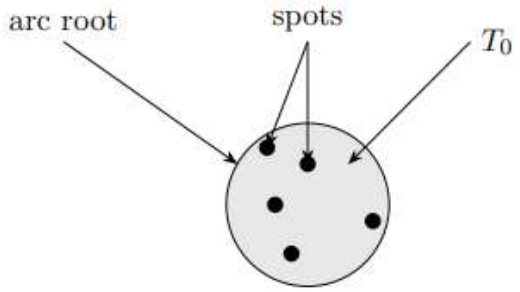

Figure 10 : Schematic representation of an arc root at the surface of a non-refractory cathode and its composition in cathode spots.

The N spots must allow a total current I_{arc} to pass. Assuming that this current is distributed uniformly, each spot carries the current $I_{spot} = I_{arc}/N$. We will first see how to determine this current I_{spot} using the cathode layer model previously introduced, which will ultimately allow us to describe the N-spot structure.

5.1. Thermal model for the spot

The heating characteristics $q(T_w, U)$ have the remarkable property of being localized in temperature T_w. This implies that a self-sustaining heating structure can only exist in the small temperature range corresponding to $q > 0$. In accordance with the work of Benilov [29, 30] we take advantage of this property by adopting the following *stationary* spot model:

- We consider the cathode as a semi-infinite medium with a temperature dependent thermal conductivity $\kappa(T)$, and a background temperature (i.e. without any spot) T_0. This means that heating processes leading to the existence of temperature T_0 are assumed to happen at length scales much larger than the spots.

- The spot is represented by a disc of temperature $T_s > T_0$ and radius r_s.
- The Joule effect in the bulk cathode is neglected.

This heat structure model is well known, and it can be shown that it evacuates by thermal conduction the power $P_{cond} = 4\, r_s\, \psi_s$, where ψ_s is the heat flow potential defined by:

$$\psi_s = \int_{T_0}^{T_s} \kappa(T)\, dT \quad (2)$$

Of course, T_s must be chosen in the interval such that $q(T_s) > 0$. For the structure to be stable [16], it is also necessary that $dq/dT_w < 0$, which means that T_s must be located in the decreasing part of the high branch of $q(T_w)$.

Assuming the sheath voltage is uniform across the surface at the value U, we can consider that the spot receives from the cathode layer the power $P_{sheath} = q(T_s, U)\ \pi\ r_s^2$. In steady state, this supplied power and the conduction losses balance each other, so that we can write the macroscopic balance:

$$P_{sheath} = P_{cond} \Rightarrow q(T_s, U)\pi r_s^2 = 4 r_s \psi_s \Rightarrow r_s = \frac{4\psi_s}{\pi q(T_s, U)} \quad (3)$$

This balance therefore makes it possible to calculate the spot radius knowing its temperature and the sheath voltage. It should be noted that this approach differs from that proposed by Benilov [30], who calculated r_s using a local energy balance at the edge of the spot, coupled with an asymptotic matching condition with the temperature disk solution. However, we will keep the proposal made in [30] consisting of fixing the temperature T_s at the maximum of the dependence $q(T_w, U)$ on T_w, for fixed U. The orders of magnitude obtained with this method remain similar to those of Benilov.

The radius and the temperature of the spot being determined, we can calculate, for a given sheath voltage U the current I_s, the power P_s and the erosion rate G_s of the spot according to the equations:

$$I_s = j(T_s, U)\pi r_s^2, \quad P_s = q(T_s, U)\pi r_s^2, \quad G_s = g(T_s, U)\pi r_s^2 \quad (4)$$

Figure 11 shows the dependencies of these quantities on the sheath voltage for various background temperatures T_0. We can see that the current per spot tends to decrease as the voltage U increases. This behavior can be interpreted as follows. From Figure 9, T_s, and therefore ψ_s, depend little on U ($T_s \sim 4100$ K), and $q(T_s, U)$ increases with U. Relation (3) then allows us to conclude that *the spot radius decreases as U increases*. Finally $j_s = j(T_s, U)$ depends little on U. Thus, $I_s = j_s\ \pi\ r_s^2$ (the current per spot) decreases.

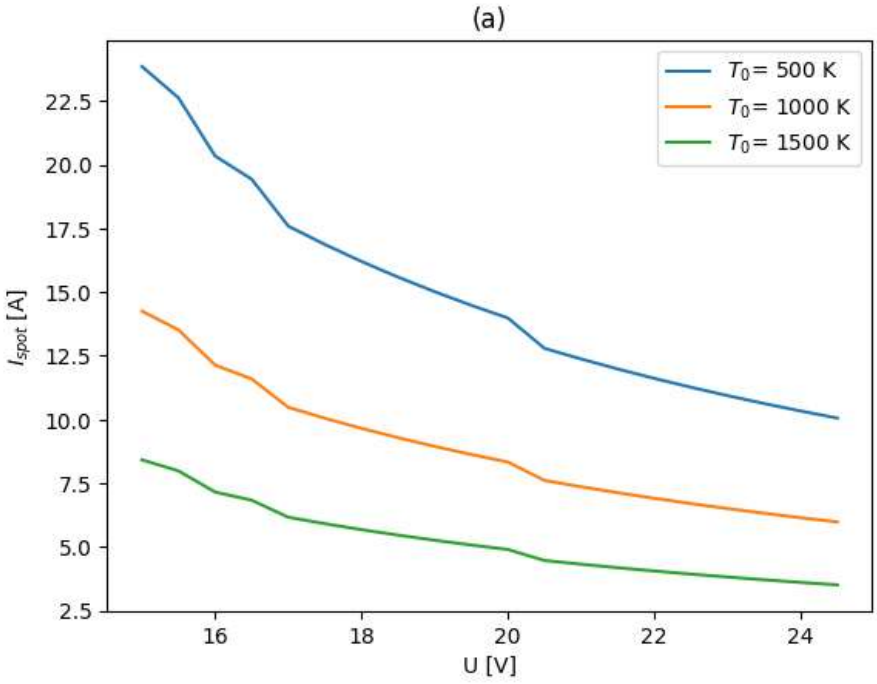

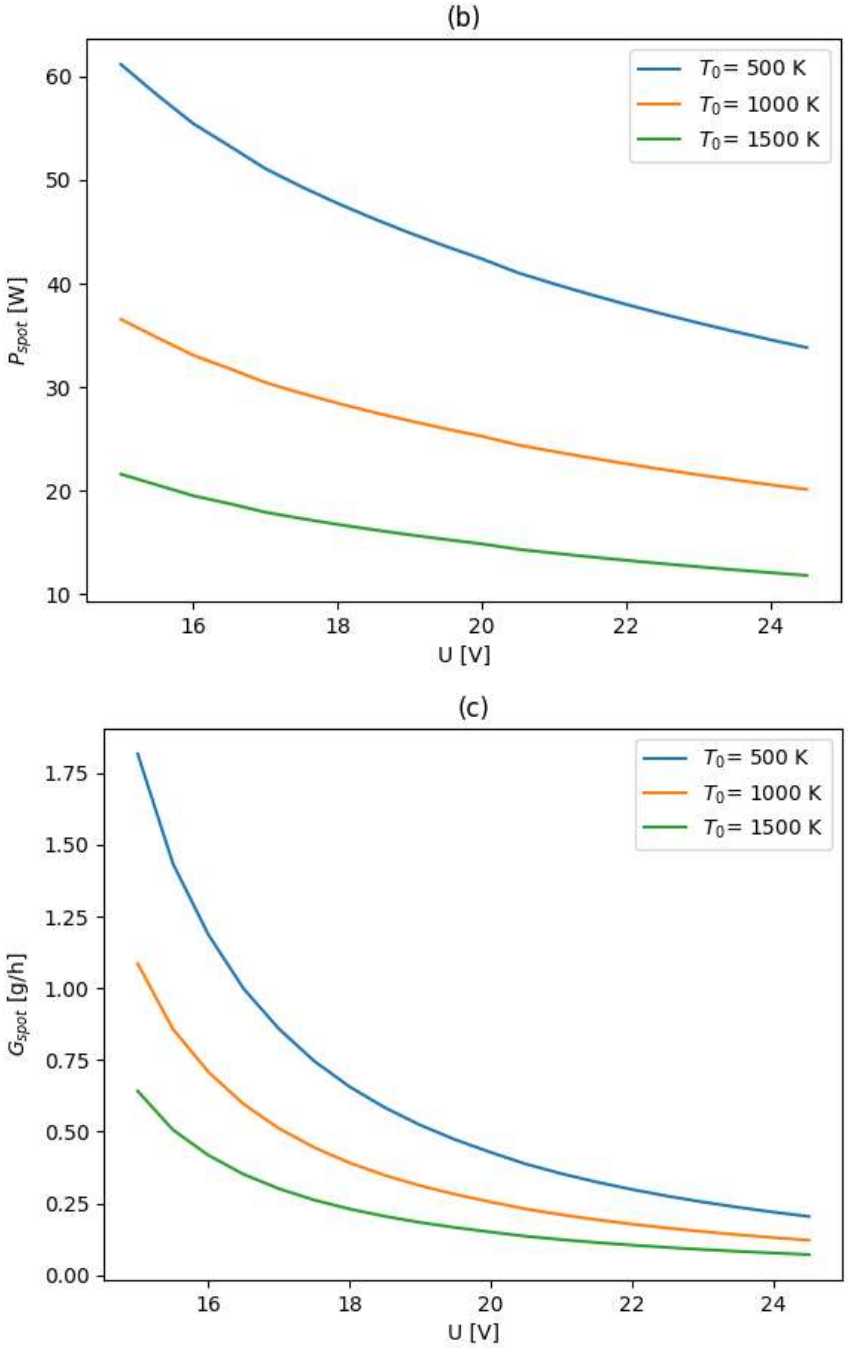

Figure 11 : Influence of the sheath voltage on (a) the current I_s, (b) the power P_s, and (c) the erosion rate G_s of a single cathode spot.

The variation of the current I_s with the background temperature T_0 can be interpreted in a similar way: a decrease in T_0 results in an increase of ψ_s, because the difference between the spot temperature and the background temperature increases. Thus, the spot radius increases, which results in an increase of I_s. The dependence of power and erosion rate can be interpreted similarly. Note that the erosion rate increases as the temperature T_0 decreases, due to the increase in the spot radius.

These results for a single spot will now be used to describe a structure with N spots.

5.2. N-spot structure of given current

The previous model allows the calculation of the characteristics of a structure with N spots (N being given) of given total current I_{arc} (in other words, we give the current per spot $I_s = I_{arc}/N$). To do this, it is sufficient to find the voltage U allowing the current I_s to be obtained. Figure 12 thus presents the evolution of the sheath voltage and the total erosion rate of the structure $G_{arc} = N\ G_s$ according to the number N of spots, for various currents I_{arc}.

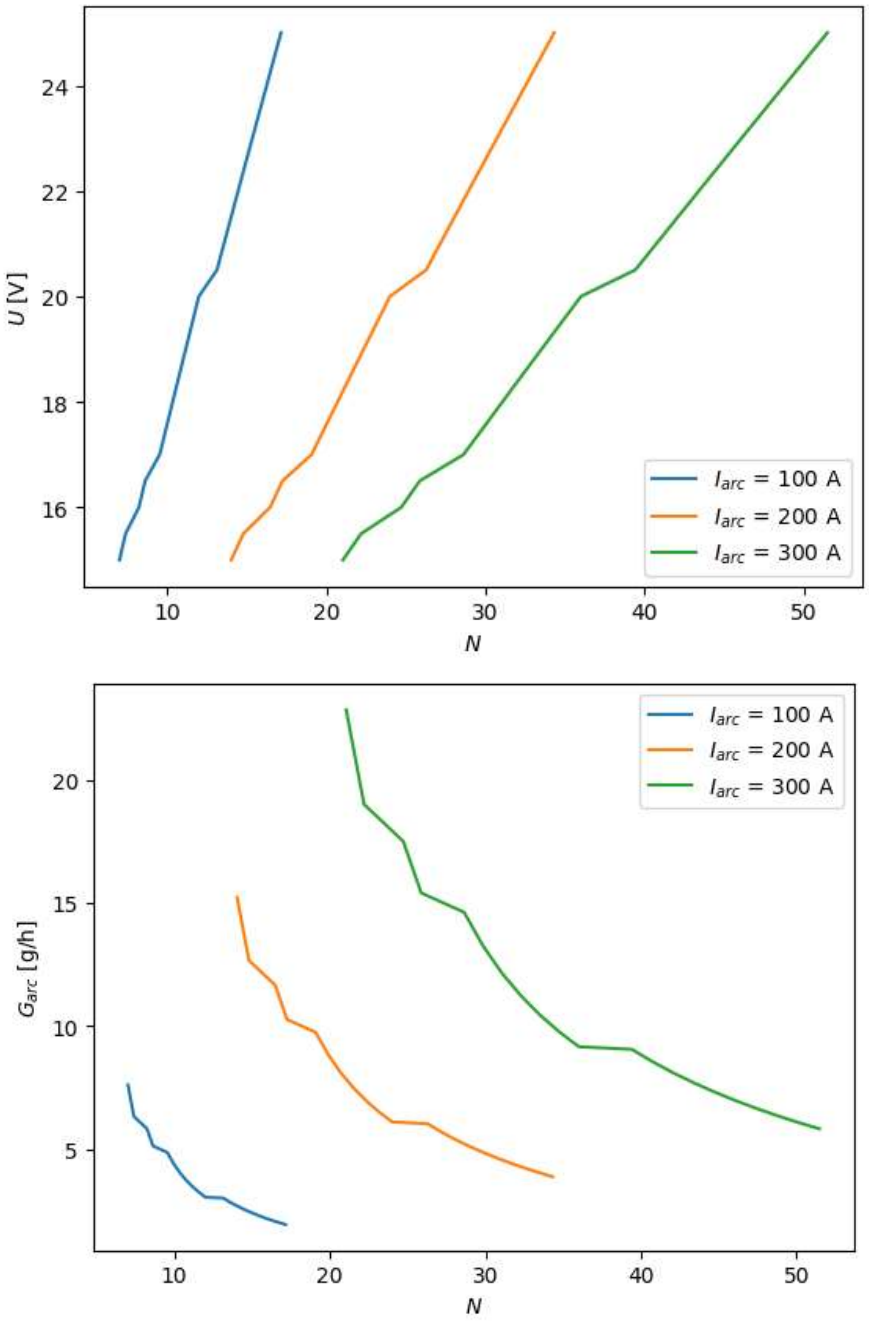

Figure 12 : Influence of the spot number N on the sheath voltage U and on the total erosion rate G_{arc} of the cathode for various current intensities I_{arc}. T_0 = 1000 K.

Note that to plot these curves, it is simpler to give U and deduce N (which leads to non-integer values of N, which are then to be excluded).

In order to test the choice of taking the temperature T_s at the maximum of the dependence of q, we studied the influence on the total erosion rate G_{arc} of the choice of this temperature in the decreasing (stable) branch of $q(T_w, U)$. The result of this study is presented in Figure 13.

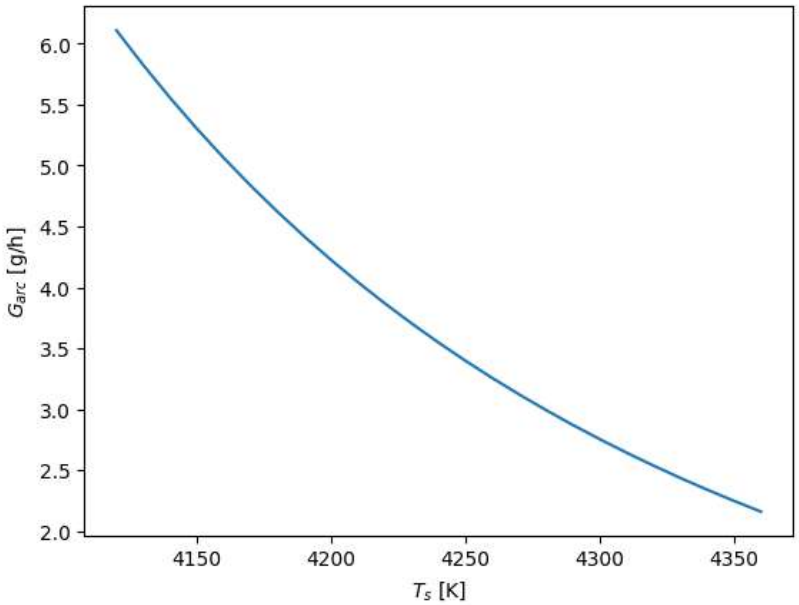

Figure 13 : Influence of the choice of surface temperature T_s on the total erosion rate G_{arc} of the cathode. I = 200 A, U = 20 V.

Let us specify that we have limited the plot to a number of spots $N \geq 1$ (this number varying with T_s). The higher the temperature T_s is chosen, the more the erosion rate G_{arc} decreases. This is due to the fact that the specific erosion $g_C = g/j$ (in g/C) fixing the erosion rate by $G_{arc} = g_C I_{arc}$ decreases with T_s (due to the increase in j). It can be shown that at fixed sheath voltage U and arc current I_{arc}, the background temperature T_0 plays no role on erosion. This seemingly counterintuitive result can be explained as follows. Once U and T_s are given, the mass flux density $g(T_s, U)$ is fixed. Moreover, $j(T_s, U)$ and I_{arc} being fixed, the total area A occupied by the spots is also fixed. Thus, the total erosion rate g(Ts, U) A is fully determined. However, if T_0 exceeds the melting temperature, a liquid phase exists on a large scale, and a significant part of the erosion then takes place by droplet emission, neglected in our model.

5.3. Application of this model at atmospheric pressure

Many industrial devices (e.g., hollow cathode plasma torches [31, 32]) use non-refractory cathodes operating in ambient gas at atmospheric pressure. Although the model [16] was developed for a vacuum arc, the vapor pressures corresponding to the surface temperatures obtained are much higher than atmospheric pressure. It can therefore be assumed that, as a first approximation, the ambient atmosphere plays a negligible role on the basic mechanisms.

We may therefore transpose the study in vacuum to the case of atmospheric pressure. With this hypothesis, the erosion rate of the cathode of a torch operating at 200 A would be (for U = 20 V) between 3 and 8 g/h (depending on the value retained for the temperature T_s, see Figure 13). This order of magnitude is in good agreement with the experimental measurements presented for example in [33]. However, the model does not explain the strong dependence of the actual erosion rate on the ambient plasma gas used. In addition, the power communicated to the cathode by the spots corresponds to only half of the experimental power reported in [33]. Taking into account the Joule effect and a possible flux due to the ambient plasma could explain these differences. Further work will therefore be necessary to clarify these points.

6. Perspectives on arc cathode interaction modeling

6.1. Refractory cathodes

The arc-refractory cathode interaction is relatively well understood. The NCPL model [23], of which many variants have been developed (e.g. [34, 35]), currently represents the best compromise between physical accuracy and implementation cost. Of course, some assumptions are questionable, such as the isothermal assumption (uniform temperatures T_e and $T_h = T_w$) in the ionization layer. The characterization of the nonequilibrium phenomena in the case of argon plasma suggests that at low electron temperatures, the ionization zone is not isothermal, since the ionization and thermalization lengths are of the same order. One can also question the role in the sheath of the emitted electrons' space charge, neglected in [23]. Indeed, the emitted electron flux constitutes an important part of the current density in steady state, and the associated electron velocity close to the cathode (thermal speed at surface temperature) is not so high, hence a potentially significant electron density.

The NCPL model has recently been extended to deal with the case of cold refractory cathodes [19, 25, 36], by adding the secondary emission phenomenon. This allows to go down to low temperature (300 K) while limiting the sheath voltage to values of the order of 150 V (for argon under 1 bar), as already noted by Cayla in previous work [34]. Such high sheath voltages imply very high electron temperatures in the ionization layer. This required a revision of the ionization layer model (previously based on the multi-fluid model [37]) to deal with the case of non-collisional atoms at high electron temperature [19]. The NCPL model is entirely decoupled from the ambient plasma. As a consequence, the cathode layer dictates its conditions to the plasma and not the other way around. This hypothesis seems questionable if an ambient plasma pre-exists in front of an initially cold cathode (which can happen in the event of displacement or jumping of the arc root).

Besides the NCPL model, one can also find a 'unified model' developed by Almeida et al. [12]. The latter has the advantage of describing all the departures from LTE (thermal, chemical, charge separation) with a single formalism. This is particularly interesting for dealing with the thermal non-equilibrium, and allows to overcome the isothermal assumption made in the NCPL model [23]. A major drawback of the unified model is that it is difficult to implement and very expensive numerically, because it must resolve both the sheath and the plasma, characterized by different length scales. Another disadvantage is that this model is based on the diffusion formalism (i.e. two temperature Stefan-Maxwell laws), and therefore assumes strongly collisional dynamics and (quasi-) Maxwellian distributions for all species. For an argon plasma, at low electron temperature, in the ionization layer, this seems correct, since we have λ_{ia}, λ_{aa}, $\lambda_{ii} << \lambda_{ion}$[d]. On the other hand, at the sheath level, most collisions are rare, and it is clear that the distribution of emitted electrons is not

Maxwellian. On this point, the NCPL model is superior, since it allows precisely to take into account these differences in collisionality, by treating the sheath and the ionization zone in two separate layers. Thus, these two approaches (unified modeling or NCPL) should be considered as complementary. Note that, from the point of view of the calculation of the characteristics $j(T_w, U)$ and $q(T_w, U)$, the two approaches give very similar results. However, only a kinetic model solving the Boltzmann equation (not developed to date) would allow to faithfully describe the entire cathode zone.

The study of heating modes of finite axisymmetric cathodes (e.g., cylindrical) in steady state is also well advanced. 2D axisymmetric modes [11, 21] have been simulated, as well as 3D modes with plane symmetry [38]. However, studies in unsteady regime are quite scarce, most of them studying the stability of steady modes [39] or transitions between modes [40].

There is no universally accepted approach to describe the coupling of the cathode layer to the ambient plasma. In general, the methodology to be adopted depends on the model used to describe this ambient plasma (depending on the nonequilibrium phenomena taken into account, see [2]). Without going into details, a main difficulty is to match the collisional description of the plasma in thermal and chemical nonequilibrium with that of the sheath, most often assumed to be non-collisional. In the case where the plasma is modeled at LTE, the coupling of the cathode zone to this plasma is even more delicate, because it is then necessary to describe the thermal relaxation (not taken into account in the NCPL model). To our knowledge, such a coupling has never been completely realized, as models based on NCPL (e.g. [13, 14]) do not describe thermal relaxation. Another example is the article [41], in which thermal relaxation is taken into account, but not ionization nonequilibrium.

6.2. Non-refractory cathodes

In this paper, we have used the model [15, 16], because it corresponds to the physics that can be deduced from the characterization of the nonequilibrium length scales. However, one can question the role of elastic ion-ion collisions, neglected in [15], and which seem to play a role at the sheath scale. Apart from this point, this cathode layer model seems physically justified, and the implementation of [16] is easily reproducible.

The thermal conduction calculation we have proposed could be improved by taking into account the Joule effect and a self-consistent local distribution of temperature and heat flux at the surface, which has already been done in the literature [17].

It should be kept in mind, however, that the model [15, 16] was developed to describe stationary spots on a locally flat surface (in the sense that its curvature radius must be small compared to the size of the sheath). It is well known that these conditions do not always reflect reality: cathode spots are nonstationary structures, moving on a surface with craters and protrusions. This complex (and unsteady) surface geometry modifies the thermal and electrical conduction in the material, and possibly the electric field in the cathode zone (field enhancement).

Consequently, spots have a life cycle with initiation and extinction phases. While extinction can be obtained from the model [15, 16], this is not the case for the initiation phases, which are generally treated by the introduction of an initial heat flux profile, imposed with an *ad hoc* distribution and duration, as in [18].

When this type of cathode is used in an ambient gas, the spots are concentrated within a 'macroscopic' arc root with a radius of around 1 mm. The surface state of the cathode is then modified by the ambient gas: for example, an oxide layer is formed if the gas contains oxygen. It has been suggested in [3] that the ambient plasma actively participates in the life cycle of the spots, at the ignition phase. This possibility should be investigated from a theoretical point of view.

Experiments are generally not able to reliably probe the small scales of spots. It therefore seems necessary to construct a more macroscopic model, based on a probabilistic approach to spot behavior, which would then allow the macroscopic arc root parameters to be predicted. Although the interest of such an approach has been known for a long time, the work carried out to date (for example [42, 43]) is often done for vacuum arcs and empirical parameters are used as a rule. A self-consistent version of such a model has not been developed to date (to our knowledge). Its development thus represents an interesting long-term challenge and would allow easier experimental validation.

7. Conclusion

In this article, we have presented a review of the most advanced work in the field of arc-cathode interaction modeling. It is convenient to organize this modeling in two steps: the study of the cathode zone, then that of the coupling of this zone with the material and, possibly, with the ambient plasma. For the first step, it is necessary to characterize the deviations from the LTE state to propose a relevant structure of the cathode zone, before any further study. The case of argon under 1 bar is now well understood. In the case of the high pressure copper plasma existing in front of a cathode spot, the presence of ionization in the sheath requires the adoption of a model taking into account the deviations from neutrality and the ionization kinetics. The model is then able to calculate the characteristics of the cathode zone $f(T_w, U)$. These characteristics are then used to calculate a cathode spot structure within the framework of a simple model (temperature disk), then a structure with N spots.

Future study perspectives were presented. The physical ingredients of arc-cathode interaction modeling are now well understood. However, it should be emphasized that the unsteady nature of the phenomena remains very little studied from a theoretical point of view. Moreover, a central challenge to be addressed in the coming years is the modeling of non-refractory cathodes in the presence of an ambient gas at atmospheric pressure. In particular, the role of the ambient plasma on the surface state (affecting the structure and dynamics of the spots) as well as on the initiation of the spots will have to be clarified.

A. Calculation of characteristic lengths of nonequilibrium phenomena

In this appendix, we describe the formalism and the raw data that are necessary for the calculation of characteristic lengths of various nonequilibrium phenomena presented in Section 2. The definitions of these lengths come for the most part from the review papers of Benilov [2, 8], and also from [19, 37, 44] (although most of them have been conceptualized much before these works).

A.1. Equilibrium composition

In the following, we will need to know the densities of electrons, ions, and atoms under conditions of chemical equilibrium at pressure p and temperatures T_e and T_h (respectively of electrons and heavy particles). For this, we use the following Saha, Dalton, and neutrality laws:

$$\frac{n_e n_i}{n_a} = K(T_e) = \frac{2Z_i}{Z_a}\left(\frac{2\pi m_e k T_e}{h^2}\right)^{3/2} \exp\left(-\frac{E_i}{k T_e}\right), \quad p = (n_a + n_i) k T_h + n_e k T_e, \quad n_e = n_i \quad (5)$$

where n_e, n_i, n_a are the electron, ion and atom densities respectively, m_e the mass of an electron, k the Boltzmann constant, and E_i the ionization energy of the atom. Multiply charged ions are not taken into account (they are assumed to form beyond the cathode region studied). We will assume that the partition functions Z_a and Z_i of atoms and ions respectively, can be approximated by the respective degeneracies g_a and g_i of the ground level [37]. The lowering of the ionization potential is negligible, as are the other Debye and Virial corrections. Useful basic data is collected in Table 1.

Element	Argon	Copper
Ionization energy E_i	15.76 eV	7.726 eV
Degeneracy g_a	1	2
Degeneracy g_i	6	1

Table 1 : Useful data for the simplified composition calculation

Combining these equations, and defining $\theta = T_e/T_h$, we obtain a quadratic equation on the electron density:

$$n_e^2 + K(T_e)(1+\theta) n_e - \frac{p K(T_e)}{k T_h} = 0 \quad (6)$$

whose (positive) solution is:

$$n_e = \frac{-b + \sqrt{\Delta}}{2}, \quad b = K(T_e)(1+\theta), \quad \Delta = b^2 + \frac{4 p K(T_e)}{k} T_h \quad (7)$$

From (7), we can deduce the densities $n_i = n_e$ and $n_a = n_e^2/K(T_e)$, as well as the average charge of heavy particles $\omega = n_i/(n_a + n_i)$, which will be useful for the cathode layer model.

A.2. Debye length

We shall use the well-known expression for the electron Debye length :

$$\lambda_D = \sqrt{\frac{\epsilon_0 k T_e}{n_e e^2}} \quad (8)$$

A.3. Thermalization length

The thermalization length of heavy particles, at which the processes of energy exchange with electrons and thermal conduction compete, is written [8]:

$$\lambda_{th}=\sqrt{\frac{\kappa_h m_h}{m_e k n_e \nu_{eh}}} \quad (9)$$

where m_h is the mass of a heavy particle (atom or ion), ν_{eh} is the electron-heavy elastic collision frequency (here assumed to be dominated by electron-ion collisions, i.e. $\nu_{eh} \sim \nu_{ei}$), and κ_h the thermal conductivity of heavy particles. The expression for ν_{ei} is well-known [45, 46] :

$$\nu_{ei}=\frac{4}{3}n_e\sqrt{\frac{8kT_e}{\pi m_e}}Q_{ei}^{(1,1)}, \quad Q_{ei}^{(1,1)}=\frac{9\pi}{2}b_{0e}^2\ln\Lambda_e, \quad b_{0e}=\frac{e^2}{12\pi\epsilon_0 kT_e}, \quad \Lambda_e=\frac{\lambda_D}{b_{0e}} \quad (10)$$

For the calculation of the thermal conductivity of heavy particles (carried out only for argon in this paper), we used the simplified formalism presented in the appendix of Almeida et al. [12]. This coefficient is written $\kappa_h = \kappa_a + \kappa_i$, with:

$$\begin{aligned}\kappa_a&=\frac{75k}{64Q_{aa}^{(2,2)}}\sqrt{\frac{\pi kT_h}{m_h}}\left(1+\frac{n_i Q_{ia}^{(2,2)}}{n_a Q_{aa}^{(2,2)}}\right)^{-1}\\ \kappa_i&=\frac{75kn_i}{64Q_{aa}^{(2,2)}n_a}\sqrt{\frac{\pi kT_h}{m_h}}\left(1+\frac{n_i Q_{ii}^{(2,2)}}{n_a Q_{ia}^{(2,2)}}\right)^{-1}\end{aligned} \quad (11)$$

where the average momentum transfer cross sections $Q^{(2,2)}$ are given by :

$$Q_{aa}^{(2,2)}[m^2]=\frac{1.12\times10^{-18}}{T_h[K]^{0.2}}, \quad Q_{ia}^{(2,2)}[m^2]=\frac{3.6\times10^{-18}}{T_h[K]^{0.3}}, \quad Q_{ii}^{(2,2)}=4\pi b_{0h}^2\ln\Lambda_h \quad (12)$$

with :

$$b_{0h}=\frac{e^2}{12\pi\epsilon_0 kT_h}, \quad \Lambda_h=\frac{\lambda_D}{b_{0h}}$$

Note that the cross sections $Q_{aa}^{(2,2)}$ and $Q_{ia}^{(2,2)}$ given here are interpolations of the Devoto tables [47], and are thus specific to argon. This is why the calculation of λ_{th} was realized only for this gas in this paper.

A.4. Mean free paths

The mean free paths of ion-atom λ_{ia}, ion-ion λ_{ii}, and atom-atom λ_{aa} collisions may be written :

$$\lambda_{ia}=\frac{1}{(n_i+n_a)Q_{ia}^{(1,1)}}, \quad \lambda_{ii}=\frac{1}{n_i Q_{ii}^{(1,1)}}, \quad \lambda_{aa}=\frac{1}{n_a Q_{aa}^{(1,1)}}, \quad (13)$$

Let us detail the expressions of cross sections $Q^{(1,1)}$. For ion-ion collisions, we have the well-known expression [45]:

$$Q_{ii}^{(1,1)} = \frac{9\pi}{2} b_{0h}^2 \ln \Lambda_h \quad (14)$$

For atom-atom collisions, in the case of argon, we have used the exponential repulsive potential presented by Devoto [47] $\phi(r) = \phi_0 \exp(-r/\rho)$ (with ϕ_0 = 7100 eV and $\rho = 2.58\ 10^{-11}$ m), and used the collision integral tables of Monchick [48] to obtain the cross section $Q_{aa}^{(1,1)}$ as:

$$Q_{aa}^{(1,1)} = 4\pi\alpha^2\rho^2 I^{(1,1)}(\alpha), \quad \alpha = \ln\left(\frac{\phi_0}{k T_h}\right) \quad (15)$$

For example, if T_h = 3000 K, $I^{(1,1)}$ = 0,22. This calculation of λ_{aa} being specific to argon, it was only realized for this gas in this paper.
Finally, ion-atom collision cross-sections $Q_{ia}^{(1,1)}$ are assumed to be dominated by charge exchange processes. Under this hypothesis, we may use the following interpolation formula [37] :

$$Q_{ia}^{(1,1)} = 2(a - b\ln(2 k T_h[eV]))^2 \quad (16)$$

where the coefficients a and b are tabulated by Anders [49]. These coefficients for the case of argon and copper, are gathered in Table 2.

Element	Argon	Copper
a[m]	$6.9\ 10^{-10}$	$1.3\ 10^{-9}$
b[m]	$9.7\ 10^{-11}$	$1.4\ 10^{-10}$

Table 2 : Useful data for the calculation of ion-atom cross sections

A.5. Ionization lengths

The ionization length for non-collisional atoms may be written (for a half-maxwellian distribution with temperature T_h) [19]:

$$\lambda_{ion}^{nc} = \sqrt{\frac{2 k T_h}{\pi m_h}} \frac{1}{k_i n_e} \quad (17)$$

where k_i is the ionization coefficient. Note that $1/k_i n_e$ represents the average lifetime of an atom in the electron gas. In the collisional regime, the diffusion of atoms on ions should be accounted for. In that case, the ionization length reads :

$$\lambda_{ion}^{d} = \sqrt{\frac{D_{ia}}{k_i n_e}}, \quad D_{ia} = \frac{3\pi}{8}\sqrt{\frac{k T_h}{\pi m_h}}\lambda_{ia} \quad (18)$$

where the mean free path λ_{ia} is the same as before. There is also a formulation that accounts for ambipolar diffusion [44] (not taken into account in this paper).

The ionization coefficient of atoms k_i may be calculated according to the method described in [37]. Two contributions (direct k_{dir} and stepwise k_{step}) are taken into account, so that $k_i = k_{dir} + k_{step}$. These two coefficients are given by :

$$k_{dir} = c_i \sqrt{\frac{8\,k\,T_e}{\pi\,m_e}} \left(E_i + 2k\,T_e\right) \exp\left(-\frac{E_i}{k\,T_e}\right) \quad (19)$$

where c_i is the derivative of the cross section at the threshold and :

$$k_{step}^{-1} = k_1^{-1} + k_2^{-1} \frac{4}{3\sqrt{\pi}} \Gamma\left(\frac{5}{2}, \frac{E_i - \Delta E}{k\,T_e}\right) \quad (20)$$

where Γ is the lower incomplete gamma function, and where :

$$k_1[m^3/s] = 4.3\times10^{-14} \left(\frac{k\,T_e}{Ry}\right)^{0.7} \left(\frac{\Delta E}{Ry}\right)^{-2.2} \exp\left(-\frac{\Delta E}{k\,T_e}\right) \quad (21)$$

$$k_2[m^3/s] = 1.3\times10^{-14} \frac{g_i}{g_a} \left(\frac{Ry}{k\,T_e}\right)^{3} \exp\left(-\frac{E_i}{k\,T_e}\right) \quad (22)$$

where Ry = 13.6 eV is Rydberg's constant, and ΔE is the energy of the first excited Russel-Saunders term, measured from the ground state. In reality, a term contains many sub-levels J, and these do not have exactly the same energy. Therefore, we have used an average value of the energies E_J of these sub-levels, weighted by their degeneracies g_J:

$$\Delta E = \frac{\sum_J g_J E_J}{\sum_J g_J} \quad (23)$$

Useful data for the calculation of ionization coefficients of argon and copper atoms are given in Tables 1 and 3. They are mostly taken from NIST tables. The derivative c_i was taken from [37] for argon and calculated from Lotz tables [50] for copper (keeping only the 4s valence electron).

Element	Argon	Copper
Excitation energy ΔE	11.65 eV	1.49 eV
Derivative c_i	18 10^{-22} m²/eV	86.7 10^{-22} m²/eV

Table 3 : Useful data for the calculation of ionization coefficients.

B. Formulation of the cathode layer model for a non-refractory cathode

Heated at temperature T_w, the cathode emits a vapor flux J_V characterized by the density n_{aw} and the average velocity v_a along x (coordinate normal to the cathode surface), given by :

$$v_a=\sqrt{\frac{2kT_w}{\pi m_a}},\quad n_{aw}=\frac{p_{vap}}{kT_w},\quad J_v=n_{aw}v_a \quad (24)$$

where k is Boltzmann's constant, m_a the mass of an emitted atom, p_{vap} the saturated vapor pressure at temperature T_w given by the Clausius-Clapeyron equation (1). The plasma is then characterized by two temperatures T_w and T_e and by its pressure p_{vap}. Under these thermodynamic conditions, one can estimate the average charge of heavy particles ω using ionization equilibrium relations (Saha, Dalton, neutrality), which are verified at the sheath edge. One can then calculate the characteristics of the potential profile, using the fit formulae given by Almeida et al. [16] :

$$\phi_\infty=-0.84-\frac{0.42\alpha_w^{3/2}}{(\alpha_w+5)(\sqrt{\alpha_w}+3)},\quad \psi_{iw}=\frac{-0.5+0.3\sqrt{\alpha_w}}{1+0.3\sqrt{\alpha_w}},\quad \psi_{i\infty}=\frac{-0.3}{1+(\alpha_w+1)^{1/3}} \quad (25)$$

where α_w measures the ratio of the Debye length to the ionization length and is defined by :

$$\alpha_w=\omega\frac{v_a}{v_s}\left(\frac{\epsilon_0 kT_e}{n_{aw}e^2}\right)\left(\frac{k_i n_{aw}}{v_a}\right),\quad v_s=\sqrt{\frac{kT_e}{m_a}} \quad (26)$$

We may also determine the atom density at the potential maximum $n_a(0)$, given by :

$$N_{aw}=\frac{n_{aw}}{n_a(0)}=\frac{4}{1+0.8\sqrt{\alpha_w}}-2+3.8\alpha_w^{1/3} \quad (27)$$

and the electric field E_w at the cathode surface :

$$E_w=\frac{kT_e}{e}\frac{k_i\omega n_{aw}}{v_s}\sqrt{\frac{2}{N_{aw}\alpha_w}}\left\{(N_{aw}-1)\sqrt{2(\chi-\phi_\infty)}\left[1+\frac{\psi_{iw}}{2(\chi-\phi_\infty)}\right]-\frac{1}{\tau}\right\}^{1/2} \quad (28)$$

where $\chi = eU/kT_e$ (U being the sheath voltage) and $\tau = 0.48$. Thanks to these intermediate variables, one can calculate the particle fluxes in current density form, using here again expressions from [16] :

$$j_{iw}=\omega J_v e\left(1-N_{aw}^{-1}\right)$$
$$j_{pl}=\frac{e}{4}\frac{\omega J_v \exp\phi_\infty}{N_{aw}\tau v_s}\sqrt{\frac{8kT_e}{\pi m_e}}\exp\left(-\frac{eU}{kT_e}\right) \quad (29)$$
$$j_{em}(T_w,E_w)=e\int_{-\infty}^{+\infty}N(T_w,\epsilon_x)D(E_w,\epsilon_x)\,d\epsilon_x$$

where j_{iw}, j_{pl} and j_{em} are respectively the ion, backscattered electrons, and emitted electrons current densities. The latter is calculated by accoring to the Murphy-Good equation (see [51] for additional

details on the expressions of N and D, and those of the numerical method used to calculate the integral). The total current density thus reads: $j = j_{iw} + j_{em} - j_{pl}$.

Using these current densities, we may build the electron energy balance equation, whose unknown is T_e, and which reads :

$$\begin{aligned} &j_{em}\left(\frac{2kT_w}{e}+U_{eff}\right)+[j_{iw}(\psi_{i\infty}-\psi_{iw})-e\,\omega J_v(\psi_{i\infty}-\phi_\infty)]\frac{kT_e}{e} \\ &=j_{pl}\left(\frac{2kT_e}{e}+U_{eff}\right)+(j+e\,\omega J_v-j_{iw})\frac{3.2kT_e}{e}+\omega J_v E_i \end{aligned} \quad (30)$$

In this equation, the effective voltage drop U_{eff} in the sheath depends on U and is given by :

$$U_{eff}=U-\frac{W-W_{eff}}{e}, \quad W_{eff}=\bar{\epsilon}-2kT_w \quad (31)$$

where ε corresponds to the mean energy variation due to the emission of an electron. This term is calculated using the method described in [28], and takes into account the Nottingham effect at low surface temperature. Once (30) has been solved for T_e we may calculate the current density $j = j_{iw} + j_{em} - j_{pl}$ and the heat flux q using :

$$\begin{aligned} q&=q_i+q_{pl}-q_{em}-q_{ev} \\ q_i&=\frac{j_{iw}}{e}[kT_e(\psi_{iw}-\phi_\infty)+eU_{eff}+E_i-W_{eff}], \quad q_{pl}=\frac{j_{pl}}{e}(2kT_e+W_{eff}) \\ q_{em}&=\frac{j_{em}}{e}(2kT_w+W_{eff}), \quad q_{ev}=\left(J_v-\frac{j_{iw}}{e}\right)(L_{vap}+2kT_w) \end{aligned} \quad (32)$$

as well as the mass flux given by :

$$g=\left(J_v-\frac{j_{iw}}{e}\right)m_a \quad (33)$$

Complément à l'article http://dx.doi.org/10.52497/jitipee.v9i1.390

C. Implicit curve tracing

A curve in the plane may be defined by an implicit equation of the form f(x, y) = 0. For example, (30) can be written $B(T_w, T_e) = 0$ for given U. Such an equation sometimes defines an explicit function y(x) but this is not always the case globally. One should therefore use a special algorithm for tracing such curves (at least by connected components). For that purpose, we have used the following method described in [52].

1) We seek for a first point on the curve. In order to achieve this, we give a first guess point (x_0, y_0) and apply the following iterations (Newton's method) :

$$y_{n+1} = y_n - \frac{f(x_0, y_n)}{\partial_y f(x_0, y_n)} \quad (34)$$

This assumes that there is at least one y such that (x_0, y) belongs to the curve.

2) Once on the curve, at point **r** = (x, y), we determine a unit tangent vector using the fact that it is perpendicular to **grad** f, and we apply a small displacement Δ along this vector. For example :

$$\boldsymbol{t} = \left(\frac{\partial_y f}{|\nabla f|}, -\frac{\partial_x f}{|\nabla f|} \right), \quad \boldsymbol{r}' = \boldsymbol{r} + \Delta \boldsymbol{t} \quad (35)$$

If necessary, the sign of **t** may be changed to reverse the sense of tracing.

3) We come back on the curve using the following Newton's method :

$$\boldsymbol{r}_{n+1} = \boldsymbol{r}_n - f(\boldsymbol{r}_n) \frac{\nabla f(\boldsymbol{r}_n)}{|\nabla f(\boldsymbol{r}_n)|^2} \quad (36)$$

4) We go back to step 2 and repeat until the whole portion of interest of the curve has been traced.

Complément à l'article http://dx.doi.org/10.52497/jitipee.v9i1.390

References

[1] I. Choquet, (2018) "Gas tungsten arc models including the physics of the cathode layer : remaining issues", Welding in the World, vol. 62, no. 1, pp. 177–196. https://doi.org/10.1007/s40194-017-0513-2
[2] M. S. Benilov, (2019) "Modeling the physics of interaction of high-pressure arcs with their electrodes : advances and challenges", Journal of Physics D : Applied Physics, vol. 53, no. 1, p. 013002.
https://doi.org/10.1088/1361-6463/ab47be
[3] B. Jüttner, (2001) "Cathode spots of electric arcs", Journal of Physics D : Applied Physics, vol. 34, no. 17, p. R103.
https://doi.org/10.1088/0022-3727/34/17/202
[4] A. Anders, (2008) "Cathodic arcs : from fractal spots to energetic condensation." Springer,. https://doi.org/10.1007/978-0-387-79108-1
[5] A. Gleizes, J.-J. Gonzalez, and P. Freton, (2005) "Thermal plasma modelling", Journal of Physics D : Applied Physics, vol. 38, no. 9, p. R153.
https://doi.org/10.1088/0022-3727/38/9/R01
[6] J. Trelles, C. Chazelas, A. Vardelle, and J. Heberlein, (2009) "Arc plasma torch modelling", Journal of thermal spray technology, vol. 18, pp. 728–752.
https://doi.org/10.1007/s11666-009-9342-1
[7] V. Rat, A. Murphy, J. Aubreton, M.-F. Elchinger, and P. Fauchais, (2008) "Treatment of nonequilibrium phenomena in thermal plasma flows", Journal of Physics D : Applied Physics, vol. 41, no. 18, p. 183001.
https://doi.org/10.1088/0022-3727/41/18/183001
[8] M. S. Benilov, (2008) "Understanding and modelling plasma–electrode interaction in high-pressure arc discharges : a review", Journal of Physics D : Applied Physics, vol. 41, no. 14, p. 144001.
https://doi.org/10.1088/0022-3727/41/14/144001
[9] E. Hantzsche, (1996), "Cathode spots - Theories of cathode spots", in Handbook of Vacuum Arc Science and Technology (R. L. Boxman, D. M. Sanders, and P. J. Martin, eds.), pp. 73–151, Park Ridge, NJ : William Andrew Publishing.
https://doi.org/10.1016/B978-081551375-9.50007-2
[10] I. Beilis, (2020) "Plasma and spot phenomena in electrical arcs", vol. 113. Springer Nature.
https://doi.org/10.1007/978-3-030-44747-2
[11] M. S. Benilov and M. Cunha, (2002) "Heating of refractory cathodes by high-pressure arc plasmas : I", Journal of Physics D : Applied Physics, vol. 35, no. 14, p. 1736. https://doi.org/10.1088/0022-3727/35/14/314
[12] N. Almeida, M. Benilov, and G. Naidis, (2008)"Unified modelling of near-cathode plasma layers in high-pressure arc discharges", Journal of Physics D : Applied Physics, vol. 41, no. 24, p. 245201
https://doi.org/10.1088/0022-3727/41/24/245201
[13] M. Lisnyak, M. D. Cunha, J. M. Bauchire, and M. S. Benilov, (2017) "Numerical modelling of high-pressure arc discharges : matching the lte arc core with the electrodes", Journal of Physics D : Applied Physics, vol. 50, no. 31, p. 315203.
https://doi.org/10.1088/1361-6463/aa76d3

[14] M. Baeva, T. Zhu, T. Kewitz, H. Testrich, and R. Foest, (2021), "Self-consistent cathode–plasma coupling and role of the fluid flow approach in torch modelling", Journal of Thermal Spray Technology, pp. 1–14.
https://doi.org/10.1007/s11666-021-01261-4
[15] M. S. Benilov and L. G. Benilova, (2010) "The double sheath on cathodes of discharges burning in cathode vapour", Journal of Physics D : Applied Physics, vol. 43, no. 34, p. 345204.
https://doi.org/10.1088/0022-3727/43/34/345204
[16] N. A. Almeida, M. S. Benilov, L. G. Benilova, W. Hartmann, and N. Wenzel, (2013), "Near-cathode plasma layer on CuCr contacts of vacuum arcs", IEEE Transactions on Plasma Science, vol. 41, no. 8, pp. 1938–1949.
https://doi.org/10.1109/TPS.2013.2260832
[17] M. S. Benilov, M. D. Cunha, W. Hartmann, S. Kosse, A. Lawall, and N. Wenzel, (2013), "Space-resolved modeling of stationary spots on copper vacuum arc cathodes and on composite CuCr cathodes with large grains", IEEE Transactions on Plasma Science, vol. 41, no. 8, pp. 1950–1958
https://doi.org/10.1109/TPS.2013.2263255
[18] H. Kaufmann, M. Cunha, M. S. Benilov, W. Hartmann, and N. Wenzel, (2017) "Detailed numerical simulation of cathode spots in vacuum arcs : Interplay of different mechanisms and ejection of droplets", Journal of Applied Physics, vol. 122, no. 16.
https://doi.org/10.1063/1.4995368
[19] M. S. Benilov, (2024), "Ionization layer with collision-free atoms at the edge of partially to fully ionized plasmas", Plasma Sources Science and Technology, vol. 33, no. 5, p. 055002.
https://doi.org/10.1088/1361-6595/ad3f49
[20] M. S. Benilov and A. Marotta, (1995), "A model of the cathode region of atmospheric pressure arcs", Journal of Physics D : Applied Physics, vol. 28, no. 9, p. 1869.
https://doi.org/10.1088/0022-3727/28/9/015
[21] M. S. Benilov and M. D. Cunha,(2003), "Bifurcation points in the theory of axially symmetric arc cathodes", Physical Review E, vol. 68, no. 5, p. 056407.
https://doi.org/10.1103/PhysRevE.68.056407
[22] D. Nandelstädt, M. Redwitz, L. Dabringhausen, J. Luhmann, S. Lichtenberg, and J. Mentel, (2002) "Determination of HID electrode falls in a model lamp III : Results and comparison with theory", Journal of Physics D : Applied Physics, vol. 35, no. 14, p. 1639.
https://doi.org/10.1088/0022-3727/35/14/304
[23] M. S. Benilov, M. Cunha, and G. Naidis, (2005) "Modelling interaction of multispecies plasmas with thermionic cathodes", Plasma Sources Science and Technology, vol. 14, no. 3, p. 517.
https://doi.org/10.1088/0963-0252/14/3/014
[24] https://fisica.uma.pt/public-domain/simulation-tools/ncpl/. Consulté le 26 février 2024.
[25] M. D. Cunha, M. A. Sargsyan, M. K. Gadzhiev, D. V. Tereshonok, and M. S. Benilov, (2023) "Numerical and experimental investigation of thermal regimes of thermionic cathodes of arc plasma torches", J. Phys. D : Appl. Phys., vol. 56, no. 39, p. 395204.
https://doi.org/10.1088/1361-6463/ace063
[26] O. Ojeda, Y. Cressault, P. Teulet, J.-P. Gonnet, D. F. N. Santos, M. D. Cunha, and M. S. Benilov, (2023) "LTE modelling of a DC arc ignition on cold electrodes", in 23rd Int. Conf. Gas Discharges and their Applications, vol. 1, pp. 64–67.
[27] E. L. Murphy and R. Good Jr, (1956) "Thermionic emission, field emission, and the transition region", Physical review, vol. 102, no. 6, p. 1464.
https://doi.org/10.1103/PhysRev.102.1464

[28] J. Paulini, T. Klein, and G. Simon, (1993) "Thermo-field emission and the Nottingham effect", Journal of Physics D : Applied Physics, vol. 26, no. 8, p. 1310. https://doi.org/10.1088/0022-3727/26/8/024
[29] M. S. Benilov, (1993) "Nonlinear heat structures and arc-discharge electrode spots", Physical Review E, vol. 48, no. 1, p. 506.
https://doi.org/10.1103/PhysRevE.48.506
[30] M. S. Benilov, (1998), "Maxwell's construction for non-linear heat structures and determination of radius of arc spots on cathodes", Physica Scripta, vol. 58, no. 4, p. 383.
https://doi.org/10.1088/0031-8949/58/4/015
[31] P. Freton, J. J. Gonzalez, and G. Escalier, (2009) "Prediction of the cathodic arc root behaviour in a hollow cathode thermal plasma torch", Journal of Physics D : Applied Physics, vol. 42, no. 19, p. 195205.
https://doi.org/10.1088/0022-3727/42/19/195205
[32] F. Sambou, J. J. Gonzalez, M. Benmouffok, and P. Freton, (2021) "Theoretical study of the arc motion in the hollow cathode of a dc thermal plasma torch", Journal of Physics D : Applied Physics, vol. 55, no. 2, p. 025201.
https://doi.org/10.1088/1361-6463/ac2a76
[33] L. I. Sharakhovsky, A. Marotta, and V. N. Borisyuk, (1997) "A theoretical and experimental investigation of copper electrode erosion in electric arc heaters II. the experimental determination of arc spot parameters", Journal of Physics D : Applied Physics, vol. 30, no. 14, p. 2018.
https://doi.org/10.1088/0022-3727/30/14/009
[34] F. Cayla, P. Freton, and J.-J. Gonzalez, (2008), "Arc/cathode interaction model", IEEE transactions on plasma science, vol. 36, no. 4, pp. 1944–1954.
https://doi.org/10.1109/TPS.2008.927378
[35] M. Baeva, M. S. Benilov, N. A. Almeida, and D. Uhrlandt, (2016), Novel non-equilibrium modelling of a dc electric arc in argon, J. Phys. D : Appl. Phys., vol. 49, no. 24, p. 245205.
https://doi.org/10.1088/0022-3727/49/24/245205
[36] D. Santos, N. Almeida, L. Benilova, and M. Benilov, (2024) "Model of non-equilibrium near-cathode plasma layers for simulation of ignition of high-pressure arcs on cold refractory cathodes", Journal of Physics D : Applied Physics, vol. 57, no. 40, p. 405202.
https://doi.org/10.1088/1361-6463/ad5f3c
[37] M. S. Benilov and G. V. Naidis, 1998 "Ionization layer at the edge of a fully ionized plasma," Physical Review E, vol. 57, no. 2, p. 2230.
https://doi.org/10.1103/PhysRevE.57.2230
[38] M. S. Benilov, M. Carpaij, and M. D. Cunha, (2006) "3D modelling of heating of thermionic cathodes by high-pressure arc plasmas", J. Phys. D : Appl. Phys., vol. 39, no. 10, pp. 2124– 2134.
https://doi.org/10.1088/0022-3727/39/10/024
[39] M. S. Benilov, M. D. Cunha, W. Hartmann, and N. Wenzel, (2014) "Numerical investigation of the stability of stationary solutions in the theory of cathode spots in arcs in vacuum and ambient gas", Plasma Sources Sci. Technol., vol. 23, no. 5, p. 054007.
https://doi.org/10.1088/0963-0252/23/5/054007
[40] R. Bötticher and M. Kettlitz, Dynamic mode changes of cathodic arc attachment in vertical mercury discharges, Journal of Physics D : Applied Physics, vol. 39, no. 13, p. 2715, 2006.
https://doi.org/10.1088/0022-3727/39/13/014
[41] J. J. Gonzalez, F. Cayla, P. Freton, and P. Teulet, (2009) "Two-dimensional self-consistent modelling of the arc/cathode interaction", Journal of Physics D : Applied Physics, vol. 42, no. 14, p. 145204.
https://doi.org/10.1088/0022-3727/42/14/145204

[42] E. Hantzsche, B. Juttner, H. Pursch, and J. Daalder, (1983) "On the random walk of arc cathode spots in vacuum", Journal of Physics D : Applied Physics, vol. 16, no. 9, p. L173. https://doi.org/10.1088/0022-3727/16/9/002
[43] M. D. Cunha, N. Wenzel, P. G. Almeida, W. Hartmann, and M. S. Benilov, (2019) "A simple model of distribution of current over cathodes of vacuum circuit breakers", IEEE Transactions on Plasma Science, vol. 47, no. 8, pp. 3462–3469. https://doi.org/10.1109/TPS.2019.2927794
[44] M. S. Benilov, (1999) "Analysis of ionization non-equilibrium in the near-cathode region of atmospheric-pressure arcs", Journal of Physics D : Applied Physics, vol. 32, no. 3, p.257. https://doi.org/10.1088/0022-3727/32/3/013
[45] M. Mitchner and C. H. Kruger Jr, (1973), "Partially ionized gases". John Wiley and Sons, Inc., New York.
[46] V. M. Zhdanov, (2002), "Transport processes in multicomponent plasma". CRC Press.
[47] R. Devoto, (1973), "Transport coefficients of ionized argon", Physics of Fluids, vol. 16, no. 5, pp. 616–623. https://doi.org/10.1063/1.1694396
[48] L. Monchick, Collision integrals for the exponential repulsive potential, The Physics of Fluids, vol. 2, no. 6, pp. 695–700, 1959. https://doi.org/10.1063/1.1705974
[49] A. Anders, (1990), "A formulary for plasma physics". Akademie-Verlag, Berlin.
[50] W. Lotz, (1970), "Electron-impact ionization cross-sections for atoms up to Z = 108", Zeitschrift für Physik A Hadrons and nuclei, vol. 232, no. 2, pp. 101–107. https://doi.org/10.1007/BF01393132
[51] M. S. Benilov and L. G. Benilova, (2013), "Field to thermo-field to thermionic electron emission : A practical guide to evaluation and electron emission from arc cathodes", Journal of Applied Physics, vol. 114, no. 6. https://doi.org/10.1063/1.4818325
[52] https://en.wikipedia.org/wiki/Implicit_curve. Consulté le 26 février 2025.